Journal of Orthopaedic Translation 50 (2025) 211–222

Contents lists available at ScienceDirect

Journal of Orthopaedic Translation

journal homepage: www.journals.elsevier.com/journal-of-orthopaedic-translation

Original Article

The Vitamin D-Sirt1/PGC1α Axis Regulates Bone Metabolism and Counteracts Osteoporosis

Cuicui Yang [a,1], Lulu Chen [a,1], Xiaoli Guo [a], Haijian Sun [a,b,**], Dengshun Miao [a,*]

[a] The Research Center for Bone and Stem Cells, Department of Anatomy, Histology and Embryology, Nanjing Medical University, Nanjing, China
[b] Department of Orthopedics, The Second Hospital of Shandong University, Cheeloo College of Medicine, Shandong University, Jinan, Shandong 250033, China

ARTICLE INFO

Keywords:
1,25(OH)$_2$D insufficiency
Osteoporosis
Overexpression of Sirt1
PGC1α
Resveratrol

ABSTRACT

Background: Objective: Vitamin D insufficiency is a major contributor to osteoporosis. This study aimed to elucidate the mechanisms by which the vitamin D-Sirt1/PGC1α axis regulates bone metabolism and counteracts osteoporosis induced by active vitamin D insufficiency.
Methods: Mouse models including Sirt1 transgenic (Sirt1^{Tg}), Cyp27b1$^{+/-}$ (active vitamin D deficient), and compound Sirt1^{Tg}Cyp27b1$^{+/-}$ mice were utilized. Bone parameters were assessed by radiography, micro-CT, histology, and immunohistochemistry. In vitro studies used bone marrow-derived mesenchymal stem cells (BM-MSCs). Gene and protein expression were analyzed by RT-PCR and Western blotting. Chromatin immunoprecipitation and luciferase assays investigated transcriptional regulation. Effects of resveratrol supplementation were examined.
Results: 1,25-dihydroxyvitamin D (1,25(OH)$_2$D) insufficiency caused downregulation of Sirt1 expression, leading to accelerated bone loss. Overexpression of Sirt1 in mesenchymal stem cells corrected bone loss by inhibiting oxidative stress, DNA damage, osteocyte senescence and senescence-associated secretory phenotype, promoting osteoblastic bone formation, and reducing osteoclastic bone resorption. 1,25(OH)$_2$D$_3$ transcriptionally upregulated Sirt1 expression in BM-MSCs through vitamin D receptor binding to the Sirt1 gene promoter. Resveratrol, a Sirt1 agonist, attenuated osteoporosis induced by 1,25(OH)$_2$D insufficiency by modulating the Sirt1/PGC1α axis. Sirt1 interacted with and deacetylated PGC1α, a transcriptional coactivator involved in mitochondrial biogenesis and energy metabolism. Deacetylated PGC1α mediated the effects of Sirt1 on osteogenesis, oxidative stress, and cellular senescence in BM-MSCs.
Conclusion: This study elucidated the critical role of the vitamin D-Sirt1/PGC1α axis in regulating bone metabolism and counteracting osteoporosis induced by active vitamin D insufficiency. The findings highlight the potential of this axis as a therapeutic target for the prevention and treatment of osteoporosis.

The Translational Potential of this Article: This research provides insights into the molecular mechanisms underlying vitamin D insufficiency-induced osteoporosis and identifies the vitamin D-Sirt1/PGC1α axis as a promising therapeutic target. The study demonstrates the potential of Sirt1 agonists, such as resveratrol, in preventing and treating osteoporosis associated with vitamin D insufficiency. These findings may lead to the development of novel therapeutic strategies targeting the Sirt1/PGC1α axis for osteoporosis management, addressing a significant unmet medical need. Furthermore, the elucidation of the interplay between vitamin D signaling, Sirt1, and PGC1α in bone metabolism could inform future clinical studies and personalized treatment approaches for patients with vitamin D insufficiency-related bone disorders."

1. Introduction

Osteoporosis, a progressive skeletal disorder characterized by low bone mass and microarchitectural deterioration of bone tissue, is a

* Corresponding author. The Research Center for Bone and Stem Cells, Department of Anatomy, Histology and Embryology, Nanjing Medical University, Nanjing, Jiangsu, 211166, China.
** Corresponding author. Department of Orthopedics, The Second Hospital of Shandong University, Cheeloo College of Medicine, Shandong University, Jinan, Shandong, 250033, China.
E-mail addresses: Shj94@email.sdu.edu.cn (H. Sun), dsmiao@njmu.edu.cn (D. Miao).
[1] These authors contributed equally to this work.

https://doi.org/10.1016/j.jot.2024.10.011
Received 8 July 2024; Received in revised form 16 September 2024; Accepted 31 October 2024

Table 1
Primers used in this study for real time RT-PCR.

Name	Sence sequence	Anti-Sence sequence
Sirt1	GCTGACGACTTCGACGACG	TCGGTCAACAGGAGGTTGTCT
RANKL	CAGCATCGCTCTGTTCCTGTA	CTGCGTTTTCATGGAGTCTCA
OPG	ACCCAGAAACTGGTCATCAGC	CTGCAATACACACACTCATCACT
ALP	CCAACTCTTTTGTGCCAGAGA	GGCTACATTGGTGTTGAGCTTTT
Osterix	CCCTTCTCAAGCACCAATGG	AAGGGTGGGTAGTCATTTGCATA
OCN	GCTGCCCTAAAGCCAAACTCT	AGAGGACAGGGAGGATCAAGTC
P16	CGCAGGTTCTTGGTCACTGT	TGTTCACGAAAGCCAGAGCG
P21	CCTGGTGATGTCCGACCTG	CCATGAGCGCATCGCAATC
P53	GCGTAAACGCTTCGAGATGTT	TTTTTATGGCGGGAAGTAGACTG
Runx2	GTGACACCGTGTCAGCAAAG	GGAGCACAGGAAGTTGGGAC
GAPDH	AGGTCGGTGTGAACGGATTTG	TGGATTTGGACGCATTGGTC

significant global health concern affecting millions of individuals worldwide [1]. One of the key contributing factors to the development of osteoporosis is vitamin D insufficiency, particularly the insufficiency of the biologically active form, 1,25-dihydroxyvitamin D ($1,25(OH)_2D$) [2–5]. We previously reported that in wild-type mice, bone mineral density, bone volume, and expression levels of the enzyme generating 1, $25(OH)_2D$, i.e. 25-hyroxyvitamin D-1-alpha-hydroxylase (1α-hydroxylase) (encoded by Cyp27b1), decreased with age [3]. This was accompanied by declining osteoblastic bone formation and increasing osteoclastic bone resorption. Nevertheless, these age-related skeletal alterations were more severe in mice heterozygous for Cyp27b1 gene deletion ($1\alpha(OH)ase^{+/-}$ mice), which, although not totally deficient in $1,25(OH)_2D$, had significantly lower serum $1,25(OH)_2D$ levels and tissue 1α(OH)ase levels than wild-type mice [3]. Consequently, these studies demonstrated that active vitamin D insufficiency accelerates the

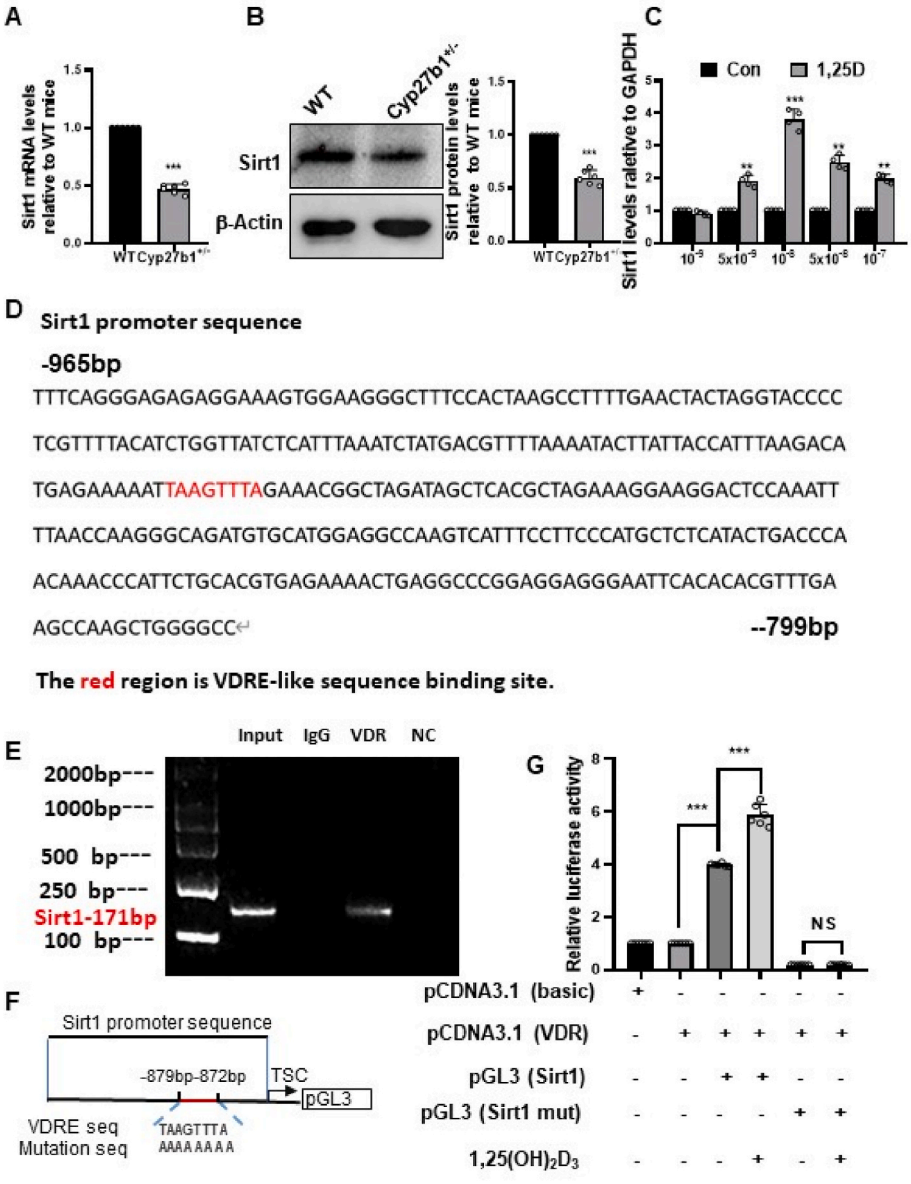

Fig. 1. $1,25(OH)_2D_3$ upregulates the transcriptional expression of Sirt1 in BM-MSCs through the VDR (A) Bar graph of the relative expression levels of Sirt1 mRNA in the thoracic vertebrae tissue of 8-month-old WT and $Cyp27b1^{+/-}$ mice; (B) Western blot detection chart and statistical chart of the relative expression levels of Sirt1 protein in the thoracic vertebrae tissue of 8-month-old WT and $Cyp27b1^{+/-}$ mice; (C) Bar graph of the relative expression levels of Sirt1 mRNA in human BM-MSCs treated with increasing concentrations of $1,25(OH)_2D_3$ for 12 h; (D) The VDR-like element (-TAAGTTTA-) motif in the Sirt1 promoter was detected by bioinformatics analysis; (E) Gel electrophoresis image of the PCR amplification products of ChIP experiment; (F) Schematic diagram of the structure of the pGL3-Sirt1 promoter reporter plasmid and the mutant pGL3-Sirt1 promoter reporter plasmid; (G) Bar graph of the experimental results of the dual luciferase reporter gene assay. **: $P < 0.01$; ***: $P < 0.001$ compared to the control group. NS: no significant difference.

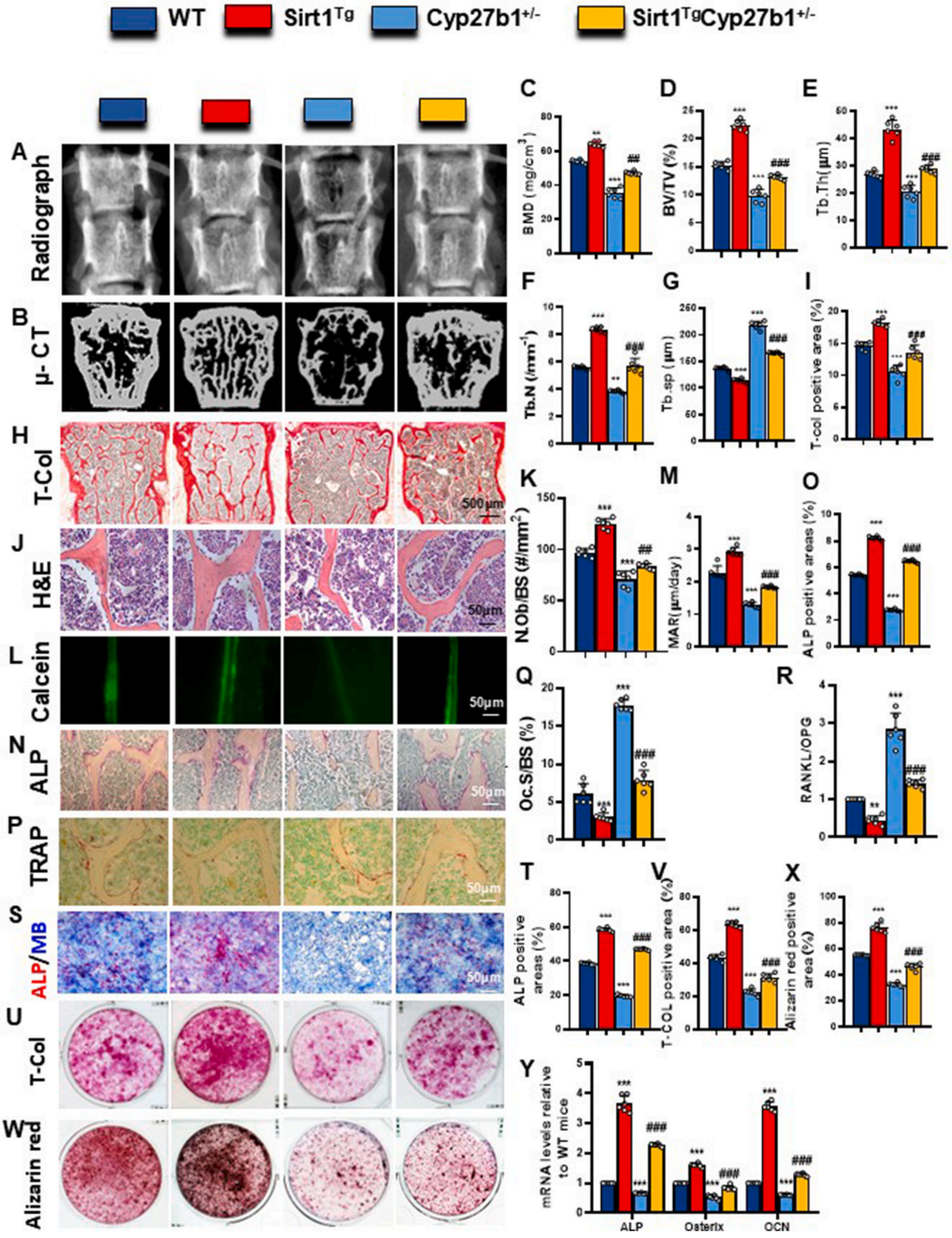

(caption on next page)

Fig. 2. Role of MSCs overexpressing Sirt1 in correcting bone loss caused by 1,25$(OH)_2$D insufficiency
(A) X-ray images of the 1st-2nd lumbar vertebrae of 8-month-old WT, Sirt1^{Tg}, Cyp27b1$^{+/-}$, and Sirt1TgCyp27b1$^{+/-}$ mice, and (B) 3D reconstruction images of the 2nd lumbar vertebrae using Micro-CT. Quantitative analysis of bone formation parameters including (C) BMD (mg/cm^3), (D) BV/TV (%), (E) Tb.Th (μm), (F) Tb.N (mm^{-1}), and (G) Tb.SP (μm); (H) Representative micrographs of T-COL immunohistochemical staining of vertebral slices, (I) Quantitative analysis of T-COL positive area (%); (J) Representative micrographs of H&E staining; (K) Number of osteoblasts (N.Ob/B.Pm., #/mm); (L) Representative micrographs of calcein green fluorescent double labeling, (M) MAR (μm/day); (N) Representative micrographs of ALP histochemical staining, (O) Quantitative analysis of ALP positive area (%); (P) Representative micrographs of TRAP histochemical staining; (Q) Quantitative analysis of osteoclast surface/bone surface; (R) Bar graphs and statistical analysis of the mRNA expression ratio of RANKL to OPG; (S) ALP/methylene blue cytochemical co-staining image of BM-MSCs derived from 8-month-old WT, Sirt1^{Tg}, Cyp27b1$^{+/-}$, and Sirt1^{Tg}Cyp27b1$^{+/-}$ mice, (T) Ratio of ALP positive cell area to methylene blue positive cell area; (U) T-Col cytochemical staining image; (V) Bar graphs and statistical analysis of the T-Col positive area; (W) Alizarin red cytochemical staining image; (×) Bar graphs and statistical analysis of the Alizarin red positive area; (Y) Bar graphs and statistical analysis of the relative mRNA expression levels of Alp, Osteris, and Ocn. Each bar graph represents the mean of 6 replicates. **: $p < 0.01$; ***: $p < 0.001$, compared with WT mice. ##: $p < 0.01$; ###: $p < 0.001$, compared with Cyp27b1$^{+/-}$ mice. (For interpretation of the references to colour in this figure legend, the reader is referred to the Web version of this article.)

progression of osteoporosis by disrupting the delicate balance between bone formation and bone resorption [6].

Extensive research efforts have been devoted to understanding the mechanisms underlying the detrimental effects of vitamin D insufficiency on bone health and exploring potential therapeutic strategies to prevent and treat osteoporosis induced by this insufficiency. One critical pathway that has gained significant attention is the role of Sirtuin 1 (Sirt1), a nicotinamide adenine dinucleotide (NAD+)-dependent deacetylase involved in various cellular processes, including bone metabolism [7,8].

Previous studies have revealed that Sirt1 can integrate multiple upstream signals to regulate various downstream targets, resulting in inhibitory effects on osteoclastogenesis and promotion of osteoblastogenesis [9]. Notably, emerging evidence suggests that Sirt1 may act as a downstream target of the 1,25$(OH)_2D_3$/vitamin D receptor (VDR) signaling pathway, playing a crucial role in mediating the effects of active vitamin D on bone homeostasis [10–12]. However, the precise mechanisms underlying the interplay between Sirt1 and 1,25$(OH)_2D_3$/VDR in the context of osteoporosis induced by 1,25$(OH)_2$D insufficiency remain to be fully elucidated.

In addition to exploring the regulatory role of Sirt1, researchers have been investigating the potential therapeutic benefits of Sirt1 agonists, such as resveratrol, in preventing and treating osteoporosis [13,14]. Resveratrol, a natural polyphenolic compound found in various plant sources, has been shown to exhibit bone-protective effects by modulating Sirt1 activity and subsequently influencing bone metabolism [15,16]. However, the specific mechanisms by which resveratrol and Sirt1 interaction contribute to the prevention and treatment of osteoporosis induced by 1,25$(OH)_2$D insufficiency warrant further investigation.

Another key player in the regulation of bone metabolism is the peroxisome proliferator-activated receptor gamma coactivator 1-alpha (PGC1α), a transcriptional coactivator that plays a pivotal role in mitochondrial biogenesis and energy metabolism [17]. Emerging evidence suggests that PGC1α may mediate the actions of Sirt1 in regulating bone metabolism [18], potentially through its deacetylation and subsequent activation by Sirt1 [19,20]. However, the interplay between Sirt1, PGC1α, and vitamin D signaling in the context of osteoporosis induced by 1,25$(OH)_2$D insufficiency remains largely unexplored.

The present research aims to elucidate the intricate mechanisms underlying the regulation of bone metabolism by the 1,25$(OH)_2D_3$/VDR/Sirt1/PGC1α axis and its potential therapeutic implications for preventing and treating osteoporosis induced by 1,25$(OH)_2$D insufficiency. By investigating the transcriptional regulation of Sirt1 by 1,25$(OH)_2D_3$/VDR, the role of Sirt1 overexpression in mesenchymal stem cells (MSCs) in correcting bone loss caused by 1,25$(OH)_2$D insufficiency, and the potential therapeutic effects of resveratrol supplementation, this study seeks to provide valuable insights into the complex interplay between these signaling pathways and their impact on bone homeostasis.

Furthermore, by exploring the involvement of PGC1α in mediating the actions of Sirt1 on bone metabolism, this research endeavors to unravel the mechanistic underpinnings of how Sirt1 and its downstream effectors modulate osteogenesis, oxidative stress, and cellular senescence in the context of 1,25$(OH)_2$D insufficiency-induced osteoporosis. Ultimately, the findings from this comprehensive study hold the potential to inform the development of novel therapeutic strategies targeting the Sirt1/PGC1α axis for the prevention and treatment of osteoporosis associated with 1,25$(OH)_2$D insufficiency, addressing a significant unmet medical need.

2. Materials and methods

2.1. Animal experiments

Three types of mutant mouse models were utilized in this study. Firstly, Sirt1^{Tg} mice were employed. These are transgenic mice that express significantly elevated levels of Sirt1 under the control of the 2.4 kb Prx1 promoter which directs overexpression of Sirt1 in mesenchymal stem cells (MSCs) [21].The generation and genotyping of these mice were conducted in our laboratory and have been previously described [21]. Secondly, Cyp27b1$^{+/-}$ mice were used. These mice were generated through the breeding of heterozygous mice and were genotyped as previously reported [3]. Lastly, Sirt1^{Tg}Cyp27b1$^{+/-}$ mice were produced by crossing Sirt1^{Tg} and Cyp27b1$^{+/-}$ mice. All three strains of mice were maintained on a C57BL/6J background. The mice were housed in a pathogen-free facility, subjected to a 12-h light/dark cycle, and provided with ad libitum access to food and water. To investigate the effects of resveratrol supplementation, post-weaning wild-type (WT) and Cyp27b1$^{+/-}$ mice were allocated to either a normal diet or a diet supplemented with 0.2 % w/w resveratrol until they reached 8 months of age [22]. Eight-month-old male WT, Sirt1^{Tg}, Cyp27b1$^{+/-}$, and Sirt1^{Tg}Cyp27b1$^{+/-}$ littermates were included in this study. The use of all mice was approved by the Institutional Animal Care and Use Committee of Nanjing Medical University (approval number: IACUC-1802007), and they were maintained in the SPF Laboratory Animal Center of Nanjing Medical University.

2.2. Radiography and micro-computed tomography

Radiographic images of tibiae and lumbar vertebrae were obtained using a Faxitron X-ray system (Faxitron X-Ray Corp., Wheeling, IL, USA) at 25 kV for 10 s with X-OMAT TL film (Eastman Kodak Co., Rochester, NY, USA). Micro-computed tomography (μCT) analysis was performed using a Skyscan 1172 scanner (Bruker, Kontich, Belgium). Femurs were scanned at 70 kVp and 114 μA with a 0.5 mm aluminum filter, 10.5 μm voxel size, 0.4-degree rotation step, frame averaging of 3, and 300 ms integration time over a 360-degree rotation. Image reconstruction was performed using NRecon software (version 1.7.3.1, Bruker) with 30 % beam hardening correction and ring artifact correction set to 6. Trabecular bone was analyzed in a region of interest (ROI) 1 mm below the growth plate, extending 2 mm distally in the distal femur. Segmentation used global thresholding with a visually determined, fixed threshold for all samples. Quantitative analyses were performed using CTAn software (version 1.18.8.0, Bruker), evaluating parameters including bone volume fraction (BV/TV), trabecular thickness (Tb.Th),

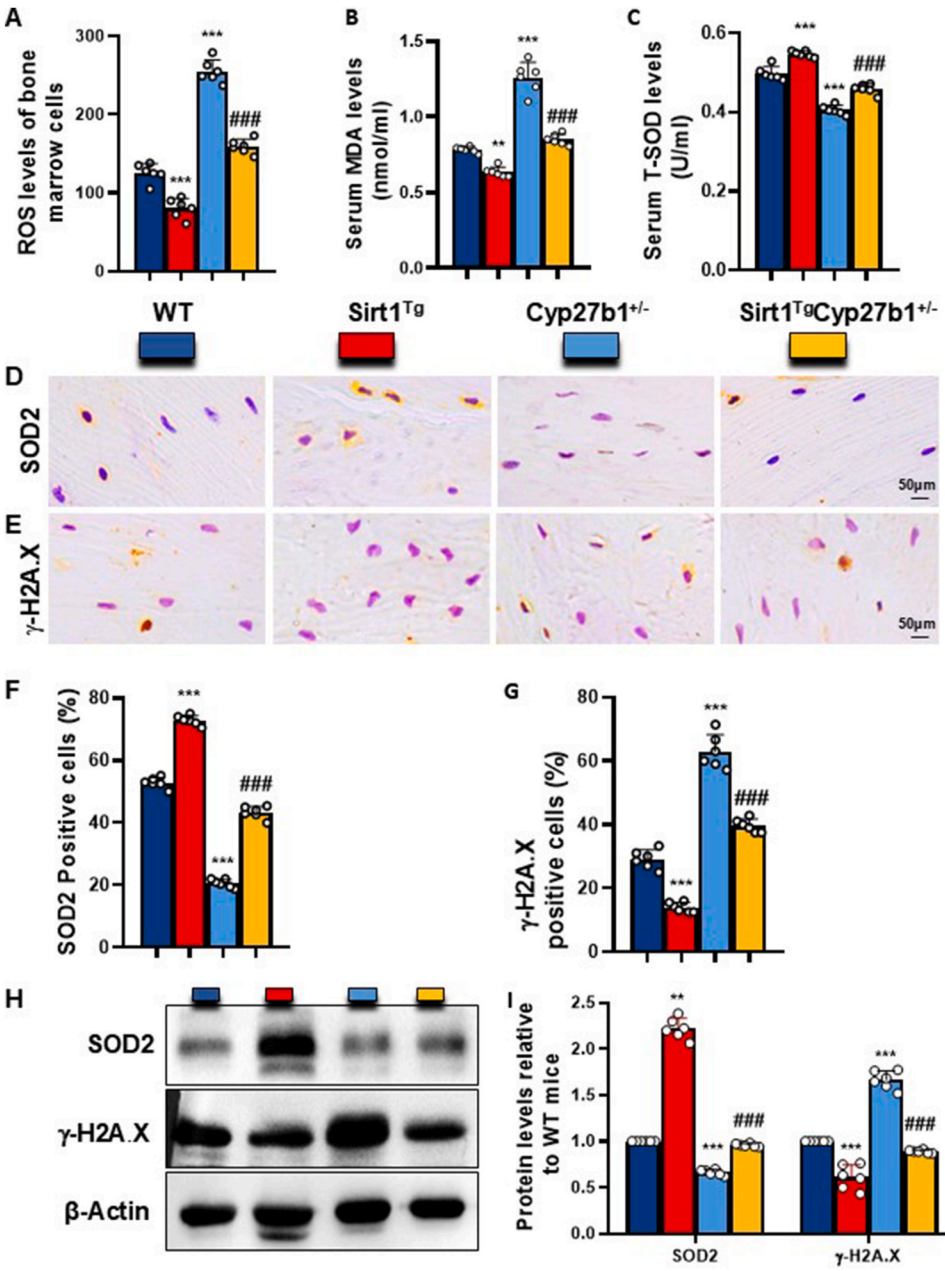

Fig. 3. Overexpression of Sirt1 in MSCs Inhibits Oxidative Stress and DNA Damage Caused by 1,25(OH)$_2$D Insufficiency
(A) Bar graph showing the level of ROS in bone marrow cells of 8-month-old WT, Sirt1^{Tg}, Cyp27b1$^{+/-}$, and Sirt1^{Tg}Cyp27b1$^{+/-}$ mice; (B) Bar graph showing the level of serum MDA; (C) Bar graph showing the level of serum T-SOD; (D) Representative micrographs of SOD2 immunohistochemical staining in vertebral slices; (E) Representative micrographs of γ-H2A.X immunohistochemical staining; (F) Bar graph showing the percentage of SOD2-positive cells; (G) Bar graph showing the percentage of γ-H2A.X-positive cells; (H) Representative Western blot images of SOD2 and γ-H2A.X protein in thoracic vertebrae; (I) Bar graph showing the relative expression levels of SOD2 and γ-H2A.X protein. Each bar shows the mean of 6 replicates. *: P < 0.05; **: P < 0.01; ***: P < 0.001, compared with WT mice. #: P < 0.05; ###: P < 0.001, compared with Cyp27b1$^{+/-}$ mice.

number (Tb.N), and separation (Tb.Sp) for trabecular bone. Density calibration used hydroxyapatite phantoms (0.25 and 0.75 g/cm^3) scanned under identical conditions, and all analyses followed guidelines by Bouxsein et al. [23] for assessing rodent bone microstructure using μCT.

2.3. Histology and histochemistry

Vertebral samples were isolated and histologically processed as previously described [5]. Paraffin sections were stained for hematoxylin and eosin (H&E), and for total collagen, histochemically for ALP and TRAP as previously described [5,24].

2.4. Immunohistochemical staining

Immunohistochemical staining was conducted using the avidin-biotin-peroxidase complex technique, as previously described [5]. The sections of paraffin-embedded tissues were first dewaxed and rehydrated. To block the endogenous peroxidase activity, the sections were then incubated with 6 % hydrogen peroxide, followed by a wash with PBS (pH 7.6). Subsequently, the slides were incubated overnight at 4 °C with primary antibodies against SOD2 (NB100-1992, Novus Biologicals, Colorado, USA), γ-H2A.X (Ser139) (#80312S, Cell Signaling Technology, Beverly, MA, USA), β-gal (ab616, Abcam), IL-1β (ab9722, Abcam), and TNF-α (sc-52746, Santa Cruz Biotechnology Inc., Dallas, USA). After

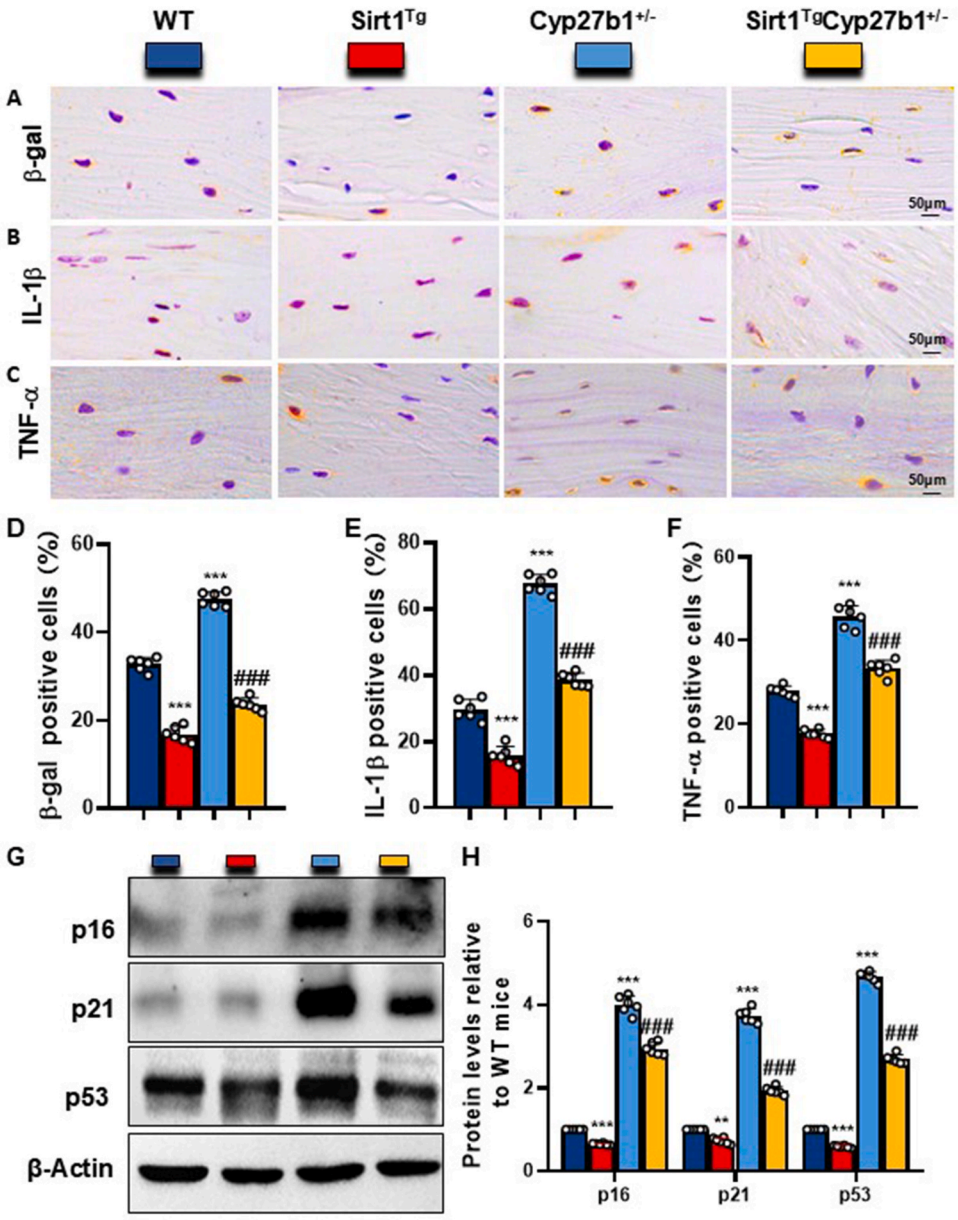

Fig. 4. Overexpression of Sirt1 in MSCs Inhibits Cellular Senescence and SASP Caused by 1,25(OH)$_2$D Insufficiency
(A) Representative micrographs of β-Gal immunohistochemical staining of vertebral slices from 8-month-old WT, Sirt1^{Tg}, Cyp27b1$^{+/-}$, and Sirt1^{Tg}Cyp27b1$^{+/-}$ mice, (B) Representative micrographs of IL-1β immunohistochemical staining, (C) Representative micrographs of TNF-α immunohistochemical staining. (D) Percentage of β-Gal-positive cells. (E) Percentage of IL-1β-positive cells. (F) Percentage of TNF-α-positive cells. (G) Representative Western blot images of p16, p21, and p53 protein expression in thoracic vertebrae. (H) Relative expression levels of p16, p21, and p53 proteins. Each bar shows the mean of 6 replicates. *: $P < 0.05$; **: $P < 0.01$; ***: $P < 0.001$, compared with WT mice. ##: $P < 0.01$; ###: $P < 0.001$, compared with Cyp27b1$^{+/-}$ mice.

a 15-min rinse with PBS, the tissues were incubated with secondary antibodies (biotinylated goat anti-rabbit IgG and goat anti-mouse IgG, Sigma). Following another wash, the sections were incubated with the Vectastain Elite ABC reagent (Vector Laboratories) for 30 min. Staining was achieved using 3,3-diaminobenzidine (2.5 mg/ml) and counterstaining was performed with Mayer's hematoxylin.

2.5. Cell cultures

Bone marrow mesenchymal stem cells (BM-MSCs) were isolated from mouse femurs and tibias and cultured as previously described [25]. After obtaining detailed informed consent, primary human BM-MSCs were isolated from bone marrow aspirates during hip replacement surgery for hip osteoarthritis treatment according to procedures approved by the Human Subjects Institutional Review Board of Nanjing Medical University. BM-MSCs were cultured in α-modified Eagle's MEM (Life Technologies) supplemented with 10 % FBS (Excell) and 1 % penicillin/streptomycin (Life Technologies) at a cell density of 10×10^6/ml. On day 3, nonadherent cells were removed using medium change and fresh medium was replaced twice per week. For osteogenic differentiation, cells were maintained in osteogenic medium (supplemented with 100 nM dexamethasone, 10 mM β-glycerophosphate, and 50 μg/ml ascorbic acid) for 21 days. Staining for alkaline phosphatase (Alp)--positive colonies (CFU-f) and Alizarin red (for mineralized nodule formation) was performed at 7 and 21 days of cultures, respectively. MitoTracker™ Staining for Mitochondria Labeling was performed as previously described [26]. SA-β-gal staining and EdU assay were performed as previously described [27]. ImageJ software was used to

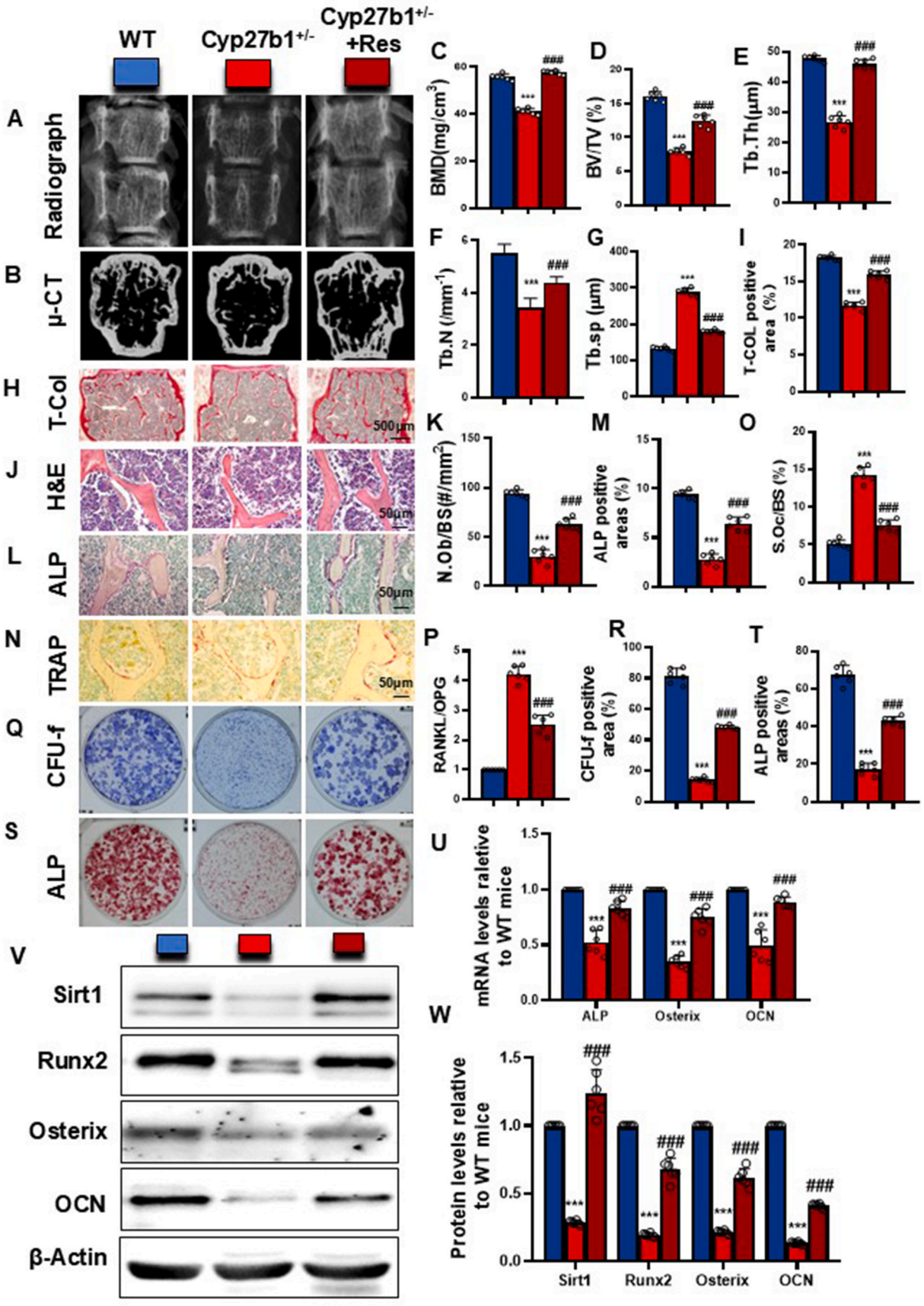

(caption on next page)

Fig. 5. The role of Sirt1 activator resveratrol supplementation in correcting osteoporosis caused by $1,25(OH)_2D$ insufficiency.
(A) X-ray images of the first and second lumbar vertebrae and (B) Micro-CT 3D reconstruction images of the second lumbar vertebrae in 8-month-old WT mice fed a normal diet and Cyp27b1$^{+/-}$ mice fed a normal or resveratrol-containing diet. Quantitative analysis results of (C) bone mineral density (BMD, mg/cm^3), (D) bone volume fraction (BV/TV, %), (E) trabecular thickness (Tb.Th, μm), and (F) trabecular separation (Tb.Sp, μm). Representative micrographs of T-COL staining on vertebral slices (G) and quantitative analysis of T-COL positive area (%) (H). Representative micrographs of H&E staining (I). Quantitative analysis of osteoblasts (N. Ob/B.Pm, #/mm) (J). Representative micrographs of ALP staining (K) and quantitative analysis of ALP positive area (%) (L). Representative micrographs of TRAP staining (M) and quantitative analysis of osteoclast surface/bone surface. (N). (O)Statistical analysis of relative expression levels of RANKL and OPG mRNA. Isolation and culture of BM-MSCs derived from the three groups of mice, showing (P) representative images of methylene blue staining and (Q) statistical analysis of CFU-f positive area. (R) Representative images of ALP cell staining and (S) statistical analysis of ALP positive area. (T) Statistical analysis of relative expression levels of Alp, Osteris, and Ocn mRNA. (U) Representative Western blot images of Sirt1, Runx2, Osterix, and OCN proteins and (V) statistical analysis of relative expression levels of Sirt1, Runx2, Osterix, and OCN proteins. Each bar shows the mean of 6 replicates. ***, $P < 0.001$ compared to WT mice. ##, $P < 0.01$; ###, $P < 0.001$ compared to Cyp27b1$^{+/-}$ mice. (For interpretation of the references to colour in this figure legend, the reader is referred to the Web version of this article.)

determine areas of staining.

2.6. Real-time RT-PCR

Total RNA was extracted from the cultured BM-MSCs and vertebrae using Trizol reagent (Invitrogen) according to the manufacturer's instructions. Complementary DNA (cDNA) was synthesized using Synthesis SuperMix (Invitrogen). Real-time RT-PCR was carried out using an Agilent Real-time System. Gapdh was amplified at the same time to normalize gene expression. Each experiment was repeated three times to determine relative gene expression differences. The sequence-specific primers of human and mice are displayed in Table 1.

2.7. Western blotting

Western blotting was performed in this study to analyze protein expression levels of various target molecules. Whole cell lysates were prepared using RIPA buffer. The protein samples were then separated by SDS-PAGE and transferred onto PVDF membranes. Subsequently, the membranes were probed with specific primary antibodies against the following proteins: Sirt1 (Cell Signaling Technology), SOD2 (NB100-1992, Novus Biologicals), γ-H2A.X (#80312S, Cell Signaling Technology), p16 (Santa Cruz), p21 (Santa Cruz), p53 (Cell Signaling Technology), Runx2 (Santa Cruz), Osterix (Santa Cruz), osteocalcin (Santa Cruz), and β-actin (Cell Signaling Technology). Immunoblotting was performed using HRP-conjugated secondary antibodies. The immunoreactive bands were detected using enhanced chemiluminescence (ECL) (Bio-Rad) and subsequently analyzed using ImageJ software.

2.8. Immunoprecipitation

Whole-cell lysates were prepared from human BM-MSCs. Immunoprecipitation experiments were conducted using the Pierce™ Crosslink Magnetic IP Kit (Thermo Scientific, Waltham, MA, USA). The immunoprecipitation assay followed the manufacturer's recommendations. Proteins extracted from 2×10^6 human BM-MSCs were mixed with 1 μg of antibody and prewashed Protein A/G. The mixture was then incubated overnight. The bound antigens were eluted from the beads by boiling the samples for 10 min. Eluted samples were obtained from SDS-PAGE. Immunoblotting was performed as previously described [7]. Primary antibodies against Sirt1, PGC1α, acetylated-lysine, and β-actin (Cell Signaling Technology, Danvers, MA, USA) were used. The immunoreactive bands were visualized by ECL chemiluminescence (Amersham).

2.9. Chromatin immunoprecipitation

Human BM-MSCs were cultured to perform chromatin immunoprecipitation (ChIP) analyses of VDR recruitment by using an anti-VDR antibody (Abcam) and SimpleChIP® Enzymatic Chromatin IP Kit (Cell Signaling Technology, Danvers, MA, USA). ChIP analyses were performed as recommended by the supplier to identify the VDR recruitment. The primers used to amplify the 193bp fragment of the human Sirt1 promoter sequence using Sirt1 sense 5′- TATGGAGTCA-CAGTGTGCCAG-3′ and antisense 5′-GCGTGAGCTATCTAGCCGT-3′ primers. The PCR products were electrophoresed on 2 % agarose gels, and visualized by ethidium bromide staining.

2.10. Construction of promoter-reporter plasmids and dual-luciferase transient expression assay

To construct the effector vector, the full coding sequence of VDR was amplified and inserted into the pCDNA3.1 vector. The promoters of the Sirt1 gene were cloned into the GV238-LUC reporter vector. Additionally, two types of plasmids were created: the pGL3-Sirt1, containing the -TAAGTTTA- sequence in the promoter region of the human Sirt1 gene linked to the promoterless firefly luciferase gene, and the pGL3-Sirt1-mut, in which - TAAGTTTA - was modified to -AAAAAAAA-. Human BM-MSCs cells were seeded at a density of 100,000 cells per well in 24-well Falcon plates, with α-MEM supplemented with 10 % FBS, 24 h before the transient transfection. Plasmids were individually transfected into the wells using Opti-MEM and liposome, as per the manufacturer's protocol. Each well received pcDNA3.0-VDR and either pGL3-Sirt1 or pGL3-Sirt1-mut (with or without 10^{-8} M $1,25(OH)_2D_3$), along with 40 ng of *Renilla reniformis* luciferase. The *R. reniformis* luciferase plasmid served as a control to monitor the transfection efficiency, providing constitutive, low-level expression. After 48 h of transfection, the cells were lysed in 1 × passive lysis buffer (Promega, Madison, WI), and the collected lysates were sequentially analyzed for Firefly and Renilla luciferase activity using the Dual-Luciferase Assay Kit (Promega Corp., Madison, WI). The experimental procedures were carried out in accordance with the instructions provided by the kit manufacturer. The Firefly/Renilla ratio was calculated for each experimental treatment group based on the mean of 6 biological replicates (wells).

2.11. RNA interference and plasmid transfection

Human small interfering RNAs (siRNAs) for PGC1α and the control siRNAs (si-NC) were designed and synthesized by Invitrogen (Grand Island, NY, USA). The PGC1α plasmid and its negative control vectors were purchased from GeneChem (Shanghai, China). Lipofectamine 3000 (L3000015, Invitrogen) were used for transfection according to the manufacturer's instructions.

2.12. Intracellular ROS analysis

To analyze the intracellular ROS levels, bone marrow cells of eight-month-old WT, Sirt1^{Tg}, Cyp27b1$^{+/-}$ and Sirt1^{Tg}Cyp27b1$^{+/-}$ mice were flushed out from femurs and labeled with 5 mM DCFDA (diacetyldichlorofluorescein) in the dark for 30 min in a water bath at 37 °C, then detected with the FACS caliber flow cytometer (Becton Dickinson, Heidelberg, Germany).

2.13. Statistics

Data are presented as mean ± SEM from at least three independent

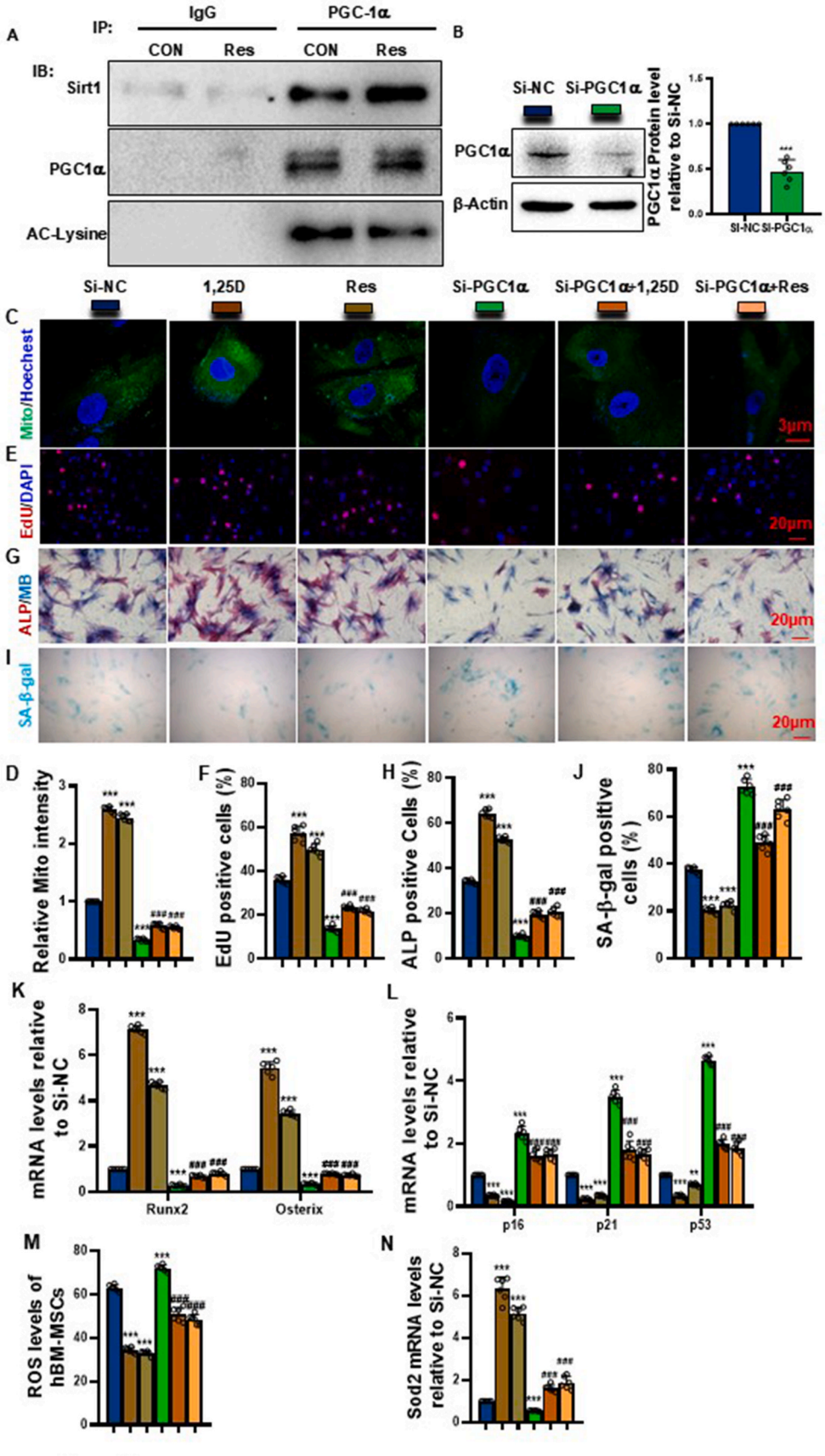

(caption on next page)

Fig. 6. Activation of the Sirt1/PGC1α pathway mediated by resveratrol promotes osteogenesis of BM-MSCs
(A) Representative image of PGC1α immunoprecipitation; (B) Efficiency of si-PGC1α plasmid transfection-mediated knockdown of PGC1α expression detected by Western blotting in human BM-MSCs; (C) Representative micrograph of mitochondria labeled with MitoTracker™ dye; (D) Statistical analysis of relative fluorescence intensity of mitochondria; (E) Representative micrograph of EdU-immunofluorescence staining in cells; (F) Percentage of EdU-positive cells; (G) Representative micrograph of double staining with methylene blue/ALP; (H) Percentage of ALP-positive cells; (I) Representative micrograph of SA-β-gal staining in cells; (J) Percentage of SA-β-gal-positive cells; (K) Statistical analysis of relative mRNA expression levels of Runx2 and Osterix; (L) Statistical analysis of relative mRNA expression levels of p16, p21, and p53; (M) Statistical analysis of ROS levels in hBM-MSCs; (N) Statistical analysis of relative mRNA expression levels of Sod-2. Each bar shows the mean of 6 replicates. **: $P < 0.01$, ***: $P < 0.001$, compared to NC; #: $P < 0.05$; ##: $P < 0.01$, ###: $P < 0.001$, compared to si-PGC1α. (For interpretation of the references to colour in this figure legend, the reader is referred to the Web version of this article.)

experiments. Differences between two groups were analyzed by two-tailed Student's t-test, and multiple groups by one-way ANOVA with post-hoc tests using GraphPad Prism 8. $P < 0.05$ was considered statistically significant.

3. Results

3.1. 1,25(OH)$_2$D$_3$ upregulates the transcriptional expression of Sirt1 in human BM-MSCs through the vitamin D receptor (VDR)

Sirt1 mRNA and protein expression levels were significantly decreased in the vertebrae of Cyp27b1$^{+/-}$ mice compared to WT mice ($p < 0.001$, Fig. 1A and B). 1,25(OH)$_2$D$_3$ upregulated the expression of the Sirt1 gene in a dose-dependent manner in human BM-MSCs, with the highest level of expression observed at the physiological concentration of 10^{-8} M ($p < 0.01$–0.001, Fig. 1C). A VDRE-like sequence was identified at position −872 in the promoter sequence of the Sirt1 gene (Fig. 1D). ChIP experiments confirmed that VDR physically binds to the Sirt1 gene promoter region (Fig. 1E). Dual-luciferase reporter gene assays showed a significant increase in luciferase activity in BM-MSCs co-transfected with pCDNA3.1-VDR and pGL3-Sirt1 plasmids ($p < 0.001$), which was further enhanced by 1,25(OH)$_2$D$_3$ treatment ($p < 0.001$). This effect was not observed with the pGL3-SIRT1-mut plasmid (Fig. 1G). These findings suggest that 1,25(OH)$_2$D$_3$ transcriptionally upregulates the expression of the SIRT1 gene in BM-MSCs through the VDR by binding to the VDRE-like sequence in the SIRT1 gene promoter region.

3.2. Role of MSCs overexpressing Sirt1 in correcting bone loss caused by 1,25(OH)$_2$D insufficiency

We next investigated whether the overexpression of the Sirt1 gene in mesenchymal stem cells (MSCs) can rectify bone loss caused by 1,25(OH)$_2$D insufficiency. For this purpose, we established a mouse model with MSCs that overexpressed Sirt1 in the Cyp27b1$^{+/-}$ background (Sirt1^{Tg}Cyp27b1$^{+/-}$). We conducted a comparison of phenotypic differences in the proximal tibiae and lumbar vertebrae of 8-month-old male mice. The results showed that Sirt1^{Tg} mice exhibited increased bone mineral density, bone volume, trabecular number, and trabecular thickness in both proximal tibiae and lumbar vertebrae compared to WT mice ($p < 0.001$ for all parameters), while trabecular separation was reduced ($p < 0.001$, Fig. 2A–G; $p < 0.01$–0.001, Supplementary Figs. 1A–F). Cyp27b1$^{+/-}$ mice showed opposite effects ($p < 0.001$ for all parameters). Sirt1^{Tg}Cyp27b1$^{+/-}$ mice demonstrated significant improvements in these parameters compared to Cyp27b1$^{+/-}$ mice ($p < 0.001$ for all parameters). Given that trabecular bone is less in the proximal metaphysis of the tibia of 8-month-old mice and more in the lumbar vertebrae of 8-month-old mice, the following analysis used the lumbar vertebrae. Sirt1^{Tg} mice showed increased total collagen staining positive area, osteoblast numbers, mineral apposition rate (MAR), and ALP-positive area ratio ($p < 0.001$ for all parameters), while Cyp27b1$^{+/-}$ mice exhibited decreases in these indicators ($p < 0.001$). Sirt1^{Tg}Cyp27b1$^{+/-}$ mice showed significant improvements compared to Cyp27b1$^{+/-}$ mice ($p < 0.001$,Fig. 2H–O). TRAP-positive osteoclast numbers and RANKL/OPG mRNA ratio decreased in Sirt1^{Tg} mice ($p < 0.001$) but increased in Cyp27b1$^{+/-}$ mice ($p < 0.001$). Sirt1^{Tg}Cyp27b1$^{+/-}$ mice showed significant reductions in these indicators compared to Cyp27b1$^{+/-}$ mice ($p < 0.001$, Fig. 2P–R). Correlation analysis showed a positive correlation between changes in osteoclast count and changes in RANKL/OPG mRNA ratio. BM-MSCs from Sirt1^{Tg} mice showed increased ALP and methylene blue-positive area, total collagen and alizarin red-positive cell area, and mRNA expression of osteogenic markers ($p < 0.001$ for all parameters). These parameters were decreased in Cyp27b1$^{+/-}$ mice but significantly improved in Sirt1^{Tg}Cyp27b1$^{+/-}$ mice ($p < 0.001$, Fig. 2S–Y). These findings suggest that the overexpression of Sirt1 in MSCs plays a crucial role in correcting the reduced osteoblastic bone formation caused by 1,25(OH)$_2$D insufficiency by enhancing the proliferation and differentiation potential of BM-MSCs.

3.3. Overexpression of Sirt1 in MSCs Inhibits Oxidative Stress and DNA Damage Caused by 1,25(OH)$_2$D insufficiency

Sirt1^{Tg} mice showed reduced levels of ROS in bone marrow cells, serum MDA, γ-H2A.X-positive osteocytes, and DNA damage-related proteins ($p < 0.01$–0.001 for all parameters). These parameters were increased in Cyp27b1$^{+/-}$ mice ($p < 0.001$) but significantly improved in Sirt1^{Tg}Cyp27b1$^{+/-}$ mice ($p < 0.001$). Conversely, SOD2-related parameters were increased in Sirt1^{Tg} mice ($p < 0.001$), decreased in Cyp27b1$^{+/-}$ mice ($p < 0.001$), and improved in Sirt1^{Tg}Cyp27b1$^{+/-}$ mice ($p < 0.001$, Fig. 3A–I). These findings suggest that the overexpression of Sirt1 in MSCs can effectively suppress oxidative stress and DNA damage, potentially contributing to melioration of the osteoporosis induced by 1,25(OH)$_2$D insufficiency.

3.4. Overexpression of Sirt1 in MSCs Inhibits Cellular Senescence and SASP caused by 1,25(OH)$_2$D insufficiency

Sirt1^{Tg} mice exhibited decreased β-gal, IL-1β, and TNF-α positive osteocytes, as well as reduced expression of p16, p21, and p53 proteins ($p < 0.05$–0.001 for all parameters). These parameters were increased in Cyp27b1$^{+/-}$ mice ($p < 0.001$) but significantly improved in Sirt1^{Tg}Cyp27b1$^{+/-}$ mice ($p < 0.001$, Fig. 4A–H). These findings suggest that MSCs overexpressing Sirt1 can effectively correct osteoporosis induced by 1,25(OH)$_2$D insufficiency by inhibiting cellular senescence and the SASP.

3.5. The role of Sirt1 agonist resveratrol supplementation in correcting osteoporosis caused by 1,25(OH)$_2$D insufficiency

Cyp27b1$^{+/-}$ + Res mice showed significant improvements in bone density, bone volume, trabecular parameters, and total collagen staining area compared to Cyp27b1$^{+/-}$ mice ($p < 0.001$ for all parameters, Fig. 5A–H). Cyp27b1$^{+/-}$ + Res mice exhibited increased osteoblast numbers, ALP-positive area, and expression of osteoblast-related genes and proteins ($p < 0.001$ for all parameters). They also showed decreased TRAP-positive osteoclast numbers and RANKL/OPG mRNA ratio ($p < 0.001$, Fig. 5I–O). Correlation analysis showed a positive correlation between changes in osteoclast count and changes in RANKL/OPG mRNA ratio. BM-MSCs from Cyp27b1$^{+/-}$ + Res mice demonstrated increased CFU-f area, ALP-positive CFU-f area, and expression of osteogenic markers compared to Cyp27b1$^{+/-}$ mice ($p < 0.001$ for all parameters,

Fig. 5P–V). These findings indicate that resveratrol, acting as a Sirt1 agonist, can promote the proliferation and osteogenic differentiation of BM-MSCs in mice with $1,25(OH)_2D$ insufficiency and correct osteogenesis disorders caused by this insufficiency.

3.6. Resveratrol-mediated activation of the Sirt1/PGC1α pathway promotes osteogenesis of BM-MSCs

Resveratrol treatment enhanced the interaction between Sirt1 and PGC1α, increased their expression levels, reduced acetyl-PGC1α level, and promoted their nuclear localization in human BM-MSCs (Fig. 6A, Supplementary Fig. 2). Western blot analysis confirmed the successful knockdown of PGC1α in human BM-MSCs ($p < 0.001$, Fig. 6B). In 1,25 $(OH)_2D_3$-treated or resveratrol-treated cells, we observed increased mitochondrial fluorescence intensity, EdU-positive cells, ALP-positive cells, and expression of osteogenic genes (*Runx2* and *Osterix*) ($p < 0.001$ for all parameters,Fig. 6C–H & K). Simultaneously, these treatments decreased SA-β-gal-positive cells, expression of aging-related genes (p16, p21, and p53) ($p < 0.01$–0.001, Fig. 6I, J & L), and ROS levels ($p < 0.001$,Fig. 6M), while increasing *SOD2* expression ($p < 0.001$,Fig. 6N). PGC1α knockdown reversed these effects, leading to decreased mitochondrial biogenesis, suppressed osteogenesis, heightened oxidative stress, and increased cellular senescence ($p < 0.001$ for all parameters). However, treatment with $1,25(OH)_2D_3$ or resveratrol partially restored these effects in PGC1α-knockdown cells ($p < 0.001$, Fig. 6C–N). These findings suggest that the Sirt1/PGC1α pathway plays a crucial role in mediating the effects of $1,25(OH)_2D_3$ and resveratrol on BM-MSC proliferation, osteogenic differentiation, and senescence.

4. Discussion

This study elucidates the critical role of the vitamin D-Sirt1/PGC1α axis in regulating bone metabolism and counteracting osteoporosis induced by active vitamin D insufficiency. Our findings demonstrate that $1,25(OH)_2D$ insufficiency leads to downregulation of Sirt1 expression, resulting in accelerated bone loss. Importantly, we show that overexpression of Sirt1 in mesenchymal stem cells can correct this bone loss through multiple mechanisms, including inhibition of oxidative stress, DNA damage, osteocyte senescence, and senescence-associated secretory phenotype, while promoting osteoblastic bone formation and reducing osteoclastic bone resorption.

A key finding of our study is the transcriptional upregulation of Sirt1 expression by $1,25(OH)_2D_3$ in bone marrow-derived mesenchymal stem cells (BM-MSCs) through vitamin D receptor (VDR) binding to the Sirt1 gene promoter. This establishes a direct link between vitamin D signaling and Sirt1 expression in the context of bone metabolism. Previous studies have suggested a relationship between vitamin D and Sirt1 in other tissues [28,29], but our work provides the first clear evidence of this regulatory mechanism in BM-MSCs and its relevance to bone homeostasis.

The protective effects of Sirt1 overexpression against $1,25(OH)_2D$ insufficiency-induced osteoporosis highlight the potential of Sirt1 as a therapeutic target. Our findings are consistent with previous studies demonstrating the bone-protective effects of Sirt1 in other contexts [30,31]. However, our work extends these findings by specifically addressing the role of Sirt1 in the context of vitamin D insufficiency, a common clinical scenario associated with osteoporosis.

Importantly, we demonstrate that resveratrol, a Sirt1 agonist, can attenuate osteoporosis induced by $1,25(OH)_2D$ insufficiency by modulating the Sirt1/PGC1α axis. This finding has significant translational potential, as resveratrol is a naturally occurring compound with a favorable safety profile [32]. Our results suggest that resveratrol supplementation could be a promising therapeutic strategy for preventing and treating osteoporosis in individuals with vitamin D insufficiency. Future clinical trials are warranted to evaluate the efficacy and optimal dosing of resveratrol in this context.

The elucidation of the interaction between Sirt1 and PGC1α in mediating the effects on osteogenesis, oxidative stress, and cellular senescence in BM-MSCs provides valuable insights into the molecular mechanisms underlying the bone-protective effects of Sirt1. Our finding that Sirt1 deacetylates PGC1α, leading to its activation, is consistent with previous studies in other tissues [20,33]. However, our work is the first to demonstrate the importance of this interaction in the context of bone metabolism and osteoporosis induced by vitamin D insufficiency.

The translational potential of our findings extends beyond the use of resveratrol. The identification of the vitamin D-Sirt1/PGC1α axis as a key regulator of bone metabolism opens up new avenues for therapeutic interventions. For instance, the development of more specific and potent Sirt1 activators could provide enhanced benefits compared to resveratrol. Several such compounds are currently in preclinical development [34], and our findings provide a strong rationale for evaluating their efficacy in osteoporosis models.

Moreover, our results suggest that combination therapies targeting both vitamin D supplementation and Sirt1 activation could have synergistic effects in preventing and treating osteoporosis. This approach could be particularly beneficial for individuals with vitamin D insufficiency who may not respond adequately to vitamin D supplementation alone. Future clinical studies should explore the potential of such combination therapies.

The role of PGC1α in mediating the effects of Sirt1 on bone metabolism also presents opportunities for therapeutic targeting. PGC1α is known to regulate mitochondrial biogenesis and energy metabolism [35], and our findings suggest that these functions may be important in maintaining bone health. Developing interventions that specifically enhance PGC1α activity in bone tissue could provide another avenue for osteoporosis treatment.

Our study also has implications for personalized medicine approaches to osteoporosis management. The variability in individual responses to vitamin D supplementation is well-documented [2], and our findings suggest that differences in Sirt1 expression or activity could contribute to this variability. Future studies should investigate whether Sirt1 genetic variants or expression levels could serve as biomarkers to predict response to vitamin D supplementation or guide treatment decisions.

The identification of the vitamin D-Sirt1/PGC1α axis as a regulator of cellular senescence and the senescence-associated secretory phenotype (SASP) in bone tissue is another important finding with translational potential. Cellular senescence has emerged as a key contributor to age-related diseases, including osteoporosis [36]. Our results suggest that targeting this axis could have senolytic effects, potentially addressing multiple aspects of age-related bone loss.

In conclusion, our study provides compelling evidence for the critical role of the vitamin D-Sirt1/PGC1α axis in regulating bone metabolism and counteracting osteoporosis induced by active vitamin D insufficiency. The elucidation of this regulatory mechanism opens up new avenues for therapeutic interventions, including the use of Sirt1 agonists like resveratrol, the development of more specific Sirt1 or PGC1α activators, and combination therapies with vitamin D supplementation. Future clinical studies should build on these findings to develop and evaluate novel treatment strategies for osteoporosis, particularly in the context of vitamin D insufficiency. Additionally, further investigation of the role of this axis in cellular senescence and the SASP could lead to interventions that address multiple aspects of age-related bone loss. Ultimately, this research contributes to our understanding of the complex interplay between vitamin D signaling, cellular metabolism, and bone homeostasis, paving the way for more effective and personalized approaches to osteoporosis prevention and treatment.

Data availability statement

All data and materials used in the study are available to any researcher for purposes of reproducing or extending the analysis.

Declaration of generative AI and AI-assisted technologies in the writing process

During the preparation of this work the authors used ChatGTP in order to improve language and readability. After using this tool, the authors reviewed and edited the content as needed and takes full responsibility for the content of the publication.

Declaration of competing interest

The authors declare no competing interests.

Acknowledgements

This work was supported by grants from the National Key R&D Program of China (2018YFA0800800), the National Natural Science Foundation of China (81730066) and the Postdoctoral Fellowship Program of CPSF (GZC20231458).

Appendix A. Supplementary data

Supplementary data to this article can be found online at https://doi.org/10.1016/j.jot.2024.10.011.

References

[1] Sozen T, Ozisik L, Basaran NC. An overview and management of osteoporosis. Eur J Rheumatol 2017;4(1):46–56.
[2] Lips P, van Schoor NM. The effect of vitamin D on bone and osteoporosis. Best Pract Res Clin Endocrinol Metabol 2011;25(4):585–91.
[3] Qiao W, Yu S, Sun H, Chen L, Wang R, Wu X, et al. 1,25-Dihydroxyvitamin D insufficiency accelerates age-related bone loss by increasing oxidative stress and cell senescence. Am J Transl Res 2020;12(2):507–18.
[4] Sun H, Qiao W, Cui M, Yang C, Wang R, Goltzman D, et al. The polycomb protein Bmi1 plays a crucial role in the prevention of 1,25(OH)2 D deficiency-induced bone loss. J Bone Miner Res 2020;35(3):583–95.
[5] Yang R, Chen J, Zhang J, Qin R, Wang R, Qiu Y, et al. 1,25-Dihydroxyvitamin D protects against age-related osteoporosis by a novel VDR-Ezh2-p16 signal axis. Aging Cell 2020;19(2):e13095.
[6] Holick MF. Vitamin D deficiency. N Engl J Med 2007;357(3):266–81.
[7] Bouras T, Fu M, Sauve AA, Wang F, Quong AA, Perkins ND, et al. SIRT1 deacetylation and repression of p300 involves lysine residues 1020/1024 within the cell cycle regulatory domain 1. J Biol Chem 2005;280(11):10264–76.
[8] Cohen-Kfir E, Artsi H, Levin A, Abramowitz E, Bajayo A, Gurt I, et al. Sirt1 is a regulator of bone mass and a repressor of Sost encoding for sclerostin, a bone formation inhibitor. Endocrinology 2011;152(12):4514–24.
[9] Chen Y, Zhou F, Liu H, Li J, Che H, Shen J, et al. SIRT1, a promising regulator of bone homeostasis. Life Sci 2021;269:119041.
[10] An BS, Tavera-Mendoza LE, Dimitrov V, Wang X, Calderon MR, Wang HJ, et al. Stimulation of Sirt1-regulated FoxO protein function by the ligand-bound vitamin D receptor. Mol Cell Biol 2010;30(20):4890–900.
[11] Chen H, Hu X, Yang R, Wu G, Tan Q, Goltzman D, et al. SIRT1/FOXO3a axis plays an important role in the prevention of mandibular bone loss induced by 1,25(OH) 2D deficiency. Int J Biol Sci 2020;16(14):2712–26.
[12] Sun W, Qiao W, Zhou B, Hu Z, Yan Q, Wu J, et al. Overexpression of Sirt1 in mesenchymal stem cells protects against bone loss in mice by FOXO3a deacetylation and oxidative stress inhibition. Metabolism 2018;88:61–71.
[13] Mobasheri A, Shakibaei M. Osteogenic effects of resveratrol in vitro: potential for the prevention and treatment of osteoporosis. Ann N Y Acad Sci 2013;1290:59–66.
[14] Rauf A, Imran M, Butt MS, Nadeem M, Peters DG, Mubarak MS. Resveratrol as an anti-cancer agent: a review. Crit Rev Food Sci Nutr 2018;58(9):1428–47.
[15] Baur JA, Sinclair DA. Therapeutic potential of resveratrol: the in vivo evidence. Nat Rev Drug Discov 2006;5(6):493–506.
[16] Deng Z, Li Y, Liu H, Xiao S, Li L, Tian J, et al. The role of sirtuin 1 and its activator, resveratrol in osteoarthritis. Biosci Rep 2019;39(5).
[17] Fernandez-Marcos PJ, Auwerx J. Regulation of PGC-1alpha, a nodal regulator of mitochondrial biogenesis. Am J Clin Nutr 2011;93(4):884S–90S.
[18] Artsi H, Gurt I, El-Haj M, Muller R, Kuhn GA, Ben Shalom G, et al. Sirt1 promotes a thermogenic gene Program in bone marrow adipocytes: from mice to (Wo)Men. Front Endocrinol 2019;10:126.
[19] Rodgers JT, Lerin C, Haas W, Gygi SP, Spiegelman BM, Puigserver P. Nutrient control of glucose homeostasis through a complex of PGC-1alpha and SIRT1. Nature 2005;434(7029):113–8.
[20] Zhou Y, Wang S, Li Y, Yu S, Zhao Y. SIRT1/PGC-1alpha signaling promotes mitochondrial functional recovery and reduces apoptosis after intracerebral hemorrhage in rats. Front Mol Neurosci 2017;10:443.
[21] Wang H, Hu Z, Wu J, Mei Y, Zhang Q, Zhang H, et al. Sirt1 promotes osteogenic differentiation and increases alveolar bone mass via Bmi1 activation in mice. J Bone Miner Res 2019;34(6):1169–81.
[22] Shakibaei M, Shayan P, Busch F, Aldinger C, Buhrmann C, Lueders C, et al. Resveratrol mediated modulation of Sirt-1/Runx2 promotes osteogenic differentiation of mesenchymal stem cells: potential role of Runx2 deacetylation. PLoS One 2012;7(4):e35712.
[23] Bouxsein ML, Boyd SK, Christiansen BA, Guldberg RE, Jepsen KJ, Muller R. Guidelines for assessment of bone microstructure in rodents using micro-computed tomography. J Bone Miner Res 2010;25(7):1468–86.
[24] Miao D, Scutt A. Histochemical localization of alkaline phosphatase activity in decalcified bone and cartilage. J Histochem Cytochem 2002;50(3):333–40 [eng].
[25] Miao D, Bai X, Panda D, McKee M, Karaplis A, Goltzman D. Osteomalacia in hyp mice is associated with abnormal phex expression and with altered bone matrix protein expression and deposition. Endocrinology 2001;142(2):926–39 [eng].
[26] Liu J, Zhang X, Chen K, Cheng Y, Liu S, Xia M, et al. CCR7 chemokine receptor-inducible lnc-Dpf3 restrains dendritic cell migration by inhibiting HIF-1alpha-Mediated glycolysis. Immunity 2019;50(3):600–615e15.
[27] Yang R, Zhang J, Li J, Qin R, Chen J, Wang R, et al. Inhibition of Nrf2 degradation alleviates age-related osteoporosis induced by 1,25-Dihydroxyvitamin D deficiency. Free Radic Biol Med 2022;178:246–61.
[28] Garcia-Martinez JM, Chocarro-Calvo A, Martinez-Useros J, Fernandez-Acenero MJ, Fiuza MC, Caceres-Rentero J, et al. Vitamin D induces SIRT1 activation through K610 deacetylation in colon cancer. Elife 2023;12.
[29] Sabir MS, Khan Z, Hu C, Galligan MA, Dussik CM, Mallick S, et al. SIRT1 enzymatically potentiates 1,25-dihydroxyvitamin D(3) signaling via vitamin D receptor deacetylation. J Steroid Biochem Mol Biol 2017;172:117–29.
[30] Zainabadi K, Liu CJ, Caldwell ALM, Guarente L. SIRT1 is a positive regulator of in vivo bone mass and a therapeutic target for osteoporosis. PLoS One 2017;12(9): e0185236.
[31] Zhou D, Ran Y, Yu R, Liu G, Ran D, Liu Z. SIRT1 regulates osteoblast senescence through SOD2 acetylation and mitochondrial dysfunction in the progression of Osteoporosis caused by Cadmium exposure. Chem Biol Interact 2023;382:110632.
[32] Faisal Z, Mazhar A, Batool SA, Akram N, Hassan M, Khan MU, et al. Exploring the multimodal health-promoting properties of resveratrol: a comprehensive review. Food Sci Nutr 2024;12(4):2240–58.
[33] Rodgers JT, Lerin C, Gerhart-Hines Z, Puigserver P. Metabolic adaptations through the PGC-1 alpha and SIRT1 pathways. FEBS Lett 2008;582(1):46–53.
[34] Bonkowski MS, Sinclair DA. Slowing ageing by design: the rise of NAD(+) and sirtuin-activating compounds. Nat Rev Mol Cell Biol 2016;17(11):679–90.
[35] Wu Z, Boss O. Targeting PGC-1 alpha to control energy homeostasis. Expert Opin Ther Targets 2007;11(10):1329–38.
[36] Foger-Samwald U, Kerschan-Schindl K, Butylina M, Pietschmann P. Age related osteoporosis: targeting cellular senescence. Int J Mol Sci 2022;23(5).